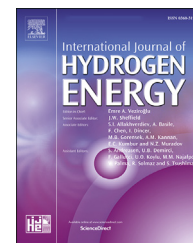


Available online at www.sciencedirect.com

ScienceDirect

journal homepage: www.elsevier.com/locate/ije

Heterostructures based on Pd–Au nanoparticles and cobalt phthalocyanine for hydrogen chemiresistive sensors

Nataliya S. Nikolaeva^a, Darya D. Klyamer^a, Sergey M. Zharkov^{b,c},
Alphiya R. Tsygankova^a, Aleksandr S. Sukhikh^a, Natalya B. Morozova^a,
Tamara V. Basova^{a,*}

^a Nikolaev Institutes of Inorganic Chemistry SB RAS, Laurentiev Pr. 3, Novosibirsk, 630090, Russia

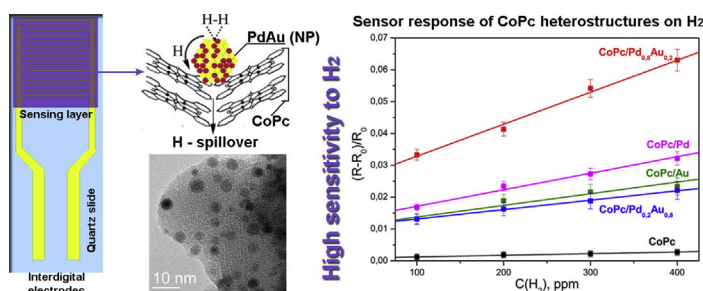
^b Kirensky Institute of Physics, Federal Research Center KSC SB RAS, Akademgorodok 50/38, Krasnoyarsk, 660036, Russia

^c Siberian Federal University, 79 Svobodny pr., Krasnoyarsk, 660041, Russia

HIGHLIGHTS

- Heterostructures based on cobalt phthalocyanine and PdAu nanoalloys were obtained.
- Effect of dilution of Pd by Au using Pd-rich or Au-rich solid solutions was studied.
- Effect of metal nanoparticles on sensor response to hydrogen was investigated.

GRAPHICAL ABSTRACT



ARTICLE INFO

Article history:

Received 12 November 2020

Received in revised form

2 March 2021

Accepted 11 March 2021

Available online 15 April 2021

Keywords:

Palladium nanoparticles

Gold nanoparticles

Bimetallic nanoparticles

Metal phthalocyanine

ABSTRACT

In this work, the effect of Pd, Au and PdAu nanoparticles on sensor response of cobalt phthalocyanine films to hydrogen was studied. For this purpose, novel heterostructures based on cobalt phthalocyanine and PdAu nanoalloys were obtained by a combination of vacuum thermal evaporation and pulsed metalorganic chemical vapor deposition (MOCVD) and investigated as active layers for hydrogen detection. The structural features and phase composition of the prepared heterostructures were studied by the techniques of X-ray diffraction, transmission electron microscopy and electron diffraction. The concentration of metal nanoparticles in the samples was determined by inductively coupled plasma atomic emission spectroscopy (ICP-AES). The chemiresistive sensor response of CoPc/M (M = Pd, Au, Pd_{0.2}Au_{0.8} and Pd_{0.8}Au_{0.2}) to hydrogen (100–400 ppm, room temperature) was compared with that of bare CoPc films. It was shown that the sensor response of the

* Corresponding author.

E-mail address: basova@niic.nsc.ru (T.V. Basova).

<https://doi.org/10.1016/j.ijhydene.2021.03.082>

0360-3199/© 2021 Hydrogen Energy Publications LLC. Published by Elsevier Ltd. All rights reserved.

Chemiresistive sensors
Hydrogen

investigated heterostructures to hydrogen (300 ppm) increased in the order CoPc (0.2%) < CoPc/Pd_{0.2}Au_{0.8} (1.9%) ~ CoPc/Au (2.2%) < CoPc/Pd (2.7%) < CoPc/Pd_{0.8}Au_{0.2} (5.6%).

© 2021 Hydrogen Energy Publications LLC. Published by Elsevier Ltd. All rights reserved.

Introduction

In recent years, hydrogen has been intensively investigated as a renewable promising energy source to replace the petroleum-based fuels [1]. Hydrogen is also used in a wide range of industries, including oil refining, chemicals, food and fertilizer production, and materials processing [2]. At the same time, hydrogen is a highly flammable and explosive gas (at a concentration of more than 4%), and for this reason, the development of sensor devices for its detection is of particular interest for ensuring industrial and environmental safety [3]. Stable and efficient sensors for the detection of hydrogen in a wide range of concentrations are required in the chemical and electronic industries, mechanical engineering, and biomedical research [4,5]. The detection of hydrogen is also an important issue for medicine. A hydrogen breath test is used as a diagnostic tool for small intestinal bacterial overgrowth and carbohydrate malabsorption, such as lactose, fructose, and sorbitol malabsorption [6]. If the level of hydrogen rises above 20 ppm, the patient is typically diagnosed as a fructose or lactose malabsorption.

Inorganic semiconductors (e.g. metal oxides, nitrides, transition metal dichalcogenide) [3,7–9], organic compounds (electroactive polymers and molecular crystals, e.g. metal phthalocyanines) [10,11], graphene and its hybrid materials [12] are often studied as active layers of chemiresistive sensors to hydrogen, however, the problem of their selectivity and sensitivity is still not completely solved, which makes the search for new materials for sensor devices an urgent task.

Although hydrogen is highly flammable at concentrations greater than 4%, lowering the sensor detection limits for hydrogen is also important to detect hydrogen leaks at the lowest possible concentration, which is necessary to prevent dangerous H₂ levels in a particular environment. There are several studies showing that the detection limit of several ppbs has been reached by using advanced methods for preparing layers of semiconductor oxides or modifying sensors with nanomaterials [13,14].

It is known that the sensitivity and selectivity of sensors can also be increased by modifying the surface of semiconductors with noble metal nanoparticles, such as Pd, Pt, and Au [15]. Many reports were devoted to the study of increased sensitivity of Pd-functionalized semiconductors due to enhanced catalytic dissociation of hydrogen on the surface of Pd nanoparticles with subsequent diffusion of the resulting atomic species onto the surface of semiconductor [4].

A variety of materials are used as active layers in chemical sensors for hydrogen detection [16]. Hydrogen gas sensors based on metal-doped semiconductor oxide layers such as SnO₂, ZnO, TiO₂, MnO₂, WO₃, etc. were the subject of discussion in several reviews [17,18]. For instance, it was shown that the

sensitivity of Pd doped (0.2%) mesoporous SnO₂ was almost ten times higher than that of pure SnO₂ (H₂ concentration was 1000 ppm at 250 °C) [19]. Toan et al. [20] also studied SnO₂ films decorated with Pd islands and found that the SnO₂ layers with the thickness of ~40 nm and Pd particles with the size of ~10 nm had maximum selectivity and sensitivity to H₂ in the concentration range from 200 to 250 ppm at 400 °C (the response time was 14 s). Sanger et al. [21] studied the sensor response of MnO₂ nanowalls covered with Pd to hydrogen in a wide concentration range from 10 to 10,000 ppm at 100 °C.

In addition to metal oxide semiconductors, carbon nanomaterials [12] and organic semiconductors have attracted considerable interest due to their quick response and regeneration, reversibility of the sensor response at room temperature, and the possibility of film deposition on flexible carriers. There are a number of examples of hybrid sensors based on metal phthalocyanines (MPc), polymers, single-walled carbon nanotubes and reduced graphene oxide doped with palladium particles in the literature [16,22,23]. For example, Pd-functionalized single-walled carbon nanotubes were used to detect hydrogen [24] and methane [25] in air at room temperature. Jaidev et al. [26] demonstrated good sensor performance of heterostructures on the basis of graphene-like carbon-wrapped carbon nanotubes decorated with dispersed platinum nanoparticles. These heterostructures showed the higher sensitivity than the corresponding single-component active layers. Organic polymers (e.g. polyaniline, polymethylmethacrylate) decorated with metal nanoparticles have also useful properties for their application in hydrogen sensors [16]. J. Hong et al. [27] prepared polymethylmethacrylate/Pd nanoparticles/single-layer graphene heterostructures exhibiting high selectivity and sensitivity to H₂ in the concentration range from 0.025 to 2%.

Metal phthalocyanines are also widely used as active layers of chemical sensors, however the works on their application for hydrogen detection are not as numerous as in the case of metal oxides and carbon nanomaterials. Metal phthalocyanines have exceptional thermal and chemical stability, versatile chemical system, and excellent processability resulting in the manufacture of thin films [28]. Unsubstituted MPcs (M = Cu, Co, Fe) are comparatively cheap commercially available dyes. Their films with controllable morphology, organization and thickness can be easily deposited by a physical vapor deposition (PVD) technique. Unlike most metal oxide sensors, the phthalocyanine-based active layers exhibit a chemoresistive sensor response at room temperature with recovery time of no more than several minutes [29,30]. These properties make the layers of metal phthalocyanines competitive with other materials mentioned above, which are used in chemiresistive sensors. Apart from this, recent studies showed that bilayer structures consisting of Pd and H₂Pc [31] or various MPc (CuPc [32], PdPc [33], VOPc [34]) demonstrated

improved sensor performance compared to that of pure phthalocyanine layers.

Another promising direction for the development of hydrogen sensors is the use of bimetallic nanoparticles. It is known that properties of bimetallic nanoparticles differ from those of their monometallic counterparts due to the synergistic effects and the changes in the surface electronic structure of nanoalloys [35,36]. Solid solutions based on palladium (PdAu, PdAg, PdCu, etc. [37,38]) were shown to have high permeability and selectivity to H₂ and increased chemical resistance to “poisoning” by CO and H₂S. Recent studies demonstrated that nanostructures based on noble metals had excellent sensor properties towards various gases. Y. Peng et al. [39] reported that the layers of reduced graphene oxide coated with PdPt nanoparticles had a repeatable and stable response to H₂ due to synergistic effects of the combination of Pt and Pd nanoparticles. Fan and co-authors [40] found that the sensitivity of ZnO nanorods doped by PtAu nanoparticles to hydrogen (250 ppm) was much higher than that of pure ZnO and ZnO with monometallic nanoparticles at the operating temperature of 250 °C.

In this work, cobalt phthalocyanine (CoPc) films were modified with Pd, Au and PdAu nanoparticles by a pulsed chemical vapor deposition method in order to enhance their sensitivity to hydrogen (100–400 ppm). The structural features and phase composition of the prepared heterostructures were studied by the techniques of X-ray diffraction, transmission electron microscopy and electron diffraction. The concentration of metal nanoparticles in the samples was determined by inductively coupled plasma atomic emission spectroscopy (ICP-AES). The effect of Pd, Au and PdAu nanoparticles on sensor response of the prepared heterostructure to hydrogen was investigated.

Experimental details

Materials and films deposition

Unsubstituted cobalt phthalocyanine was synthesized according to the technique described elsewhere [41] by heating a mixture of phthalonitrile (Sigma Aldrich) and cobalt chloride at 180 °C. CoPc: C₃₂H₁₆N₈Co. Anal. Calc: C 67.3; H 2.8; N 19.6. Found: C 67.3; H 2.7; N 19.7. IR spectrum (KBr; ω , cm⁻¹): 1609, 1591, 1522, 1468, 1425, 1333, 1288, 1165, 1121, 1088, 1001, 951, 912, 874, 779, 754, 571, 517, 434.

MOCVD precursors, [Pd(hfac)₂] (palladium(II) bis(1,1,1,5,5,5-hexafluoro-2,4-pentanedione)) and [Me₂Au(thd)] (dimethylgold(III) (2,2,6,6-tetramethyl-3,5-heptanedione)), were synthesized according to the techniques described elsewhere [42,43]. All complexes were purified by double sublimation (CoPc: P = 5 · 10⁻⁵ Torr, T = 430 °C; MOCVD precursors: P = 5 · 10⁻² Torr, T = 60–80 °C).

First, CoPc layers were deposited by vacuum thermal evaporation at P = 5 · 10⁻⁵ Torr. The evaporator temperature was 450 °C, the deposition time was 1 h, and the substrate temperature was 50 °C. Si(100), a freshly cleaved single crystal of NaCl and glass plates, as well as glass slides with interdigitated Pt electrodes (IDE, Dropsens: the gaps dimension is 10 μm; the number of digits is 125 × 2 with a digit length equal to 6760 μm; cell constant is 0.0118 cm⁻¹) were used as substrates.

After that the surface of CoPc films was decorated by Pd, Au or PdAu nanoparticles using a pulsed metal-organic chemical vapor deposition. The detailed description of the pulsed MOCVD technique has already been given in our previous publication [34]. The experimental parameters were selected based on the available data on thermal properties of the precursors: evaporator temperatures (T_{vap}) were 60–75 °C for [Pd(hfac)₂] and 60–75 °C for [Me₂Au(thd)]; the substrate temperature (T_s) was 250 °C; the ratio of buffer-gas/reactant gas (Ar/H₂) was 4:1,6; the total reactor pressure was ~8 Torr. Metal nanoparticles Pd_xAu_{1-x} (x = 0–1) were obtained by varying the evaporation temperatures and, consequently, the relative concentrations of the precursors in the reaction zone. The deposition cycle involves the following steps: evacuation of the reactor, input of the precursor, input of the buffer and reaction gases, decomposition reaction and evacuation of the reactor. The change of the pressure during the deposition cycle is shown in Fig. S1 (Supporting Information).

Films characterization

Thin film X-ray diffraction (XRD) patterns were obtained in the 2θ range from 3 to 60° using a Shimadzu XRD-7000 powder diffractometer (Cu-anode sealed tube with Ni filter, Bragg-Brentano geometry with vertical θ-θ goniometer, OneSight SSD-detector, 0.0143° step with 240 s equivalent accumulation time per data point). Al₂O₃ sample prepared as a fine layer of powder on the glass substrate surface was used as external reference standard.

The films microstructure was investigated using a scanning electron microscope JEOL-JSM 6700 F. The microstructure, phase and element compositions of samples deposited on a NaCl freshly cleaved crystal were analyzed using a transmission electron microscopy (TEM), electron diffraction, and energy dispersive spectroscopy on JEM-2100 transmission electron microscope (TEM, JEOL) equipped with an Inca x-sight energy dispersive spectrometer (Oxford). The diffraction patterns were identified using the program DigitalMicrograph (Gatan) and crystal structure database ICDD PDF 4+ (2020).

A high-resolution spectrometer iCAP 6500 (Thermo Fisher Scientific) was used for element analysis. The layer of CoPc/M (M = Pd, Au, PdAu) was washed off the surface of the substrate using a minimal amount of concentrated HCl and HNO₃ (3:1). The samples were dissolved using screw cap polypropylene tubes; the process temperature was about 100 °C. The sample solution was injected into the plasma through a nebulizer of SeaSpray type using a peristaltic pump with the rate of 0.7 mL/min. The following conditions of the analysis were used: cooling argon flow – 12 L/min, secondary – 0.5 L/min; registration time on the first slit – 15 s; registration time on the second slit – 5 s. The power supplied to an ICP inductor was 1150 W. The registration of emission spectra was carried out at the axial observation of plasma. The following reagents were used for the samples preparation: Hydrochloric acid ACS reagent, 37%, Nitric acid 70%, purified by redistillation, ≥99.999% trace metals basis; deionized water purified with the Direct-Q3 system (Millipore) > 18 MΩ/cm; high purity argon; Gold Standard for ICP TraceCERT®, 1000 mg/L Au in hydrochloric acid; Palladium Standard for ICP TraceCERT®, 1000 mg/L Pd in hydrochloric acid. To determine Au and Pd the

most intense spectral lines were used (without the spectral influence). Spectral lines for Au were 242.595 and 267.597 nm, while those for Pd were 324.270, 340.458 and 360.955 nm. The technique verification by spike experiment was provided.

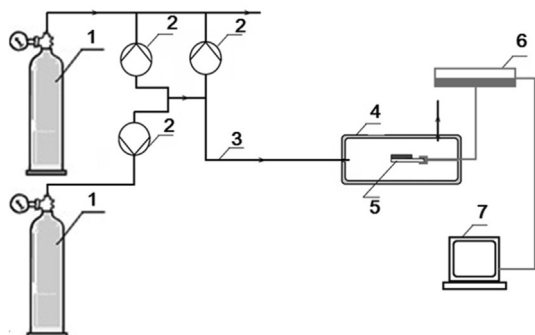
Study of sensor properties

For the investigation of chemiresistive sensor response, the heterostructures were deposited onto glass slides with interdigitated electrodes. The samples were placed in a flow cell, which was alternately injected with hydrogen of the required concentration and air. The scheme of the sensing measurement system is given in Fig. 1. Air was used as a diluent and purging gas. Pure commercial H₂ gas were used as an analyte source. The concentration of hydrogen was varied from 100 to 400 ppm. The gas-analyte was injected into the flow cell at a constant flow rate of 300 mL/min; the exposure time was 15 s. After each input of a gas-analyte the cell was purged with air. All sensor measurements were carried out at room temperature; the value of relative humidity (RH) was 10%. To study selectivity of the heterostructures their sensor response to ammonia (100 ppm), carbon dioxide (1000 ppm), ethanol (10,000 ppm) and formaldehyde (10,000 ppm) was measured at the same experimental conditions. The change in the film resistance during the introduction of hydrogen and subsequent air purging was measured using an electrometer Keithley 236. The sensor response was defined as $(R-R_0)/R_0$ (R_0 is the resistance of cobalt phthalocyanine film or CoPc-based heterostructures before H₂ injection, while R is the film resistance at a certain hydrogen concentration).

Results and discussion

Films characterization

The structure of as-deposited CoPc films and the same films after MOCVD experiments was investigated by XRD in order to study possible structural changes, since it is known that phthalocyanine films can undergo a phase transition when heated. XRD patterns for CoPc films before heating and after MOCVD experiments are shown on Fig. 2 as examples. The



1 – tanks with a gaseous analyte and purging and diluents gas (air), 2 – mass flow controllers, 3 – gas mixture with a given analyte concentration, 4 – gas cell, 5 – active layer, 6 – electrometer, 7 – computer.

Fig. 1 – Scheme of the sensing measurement system.

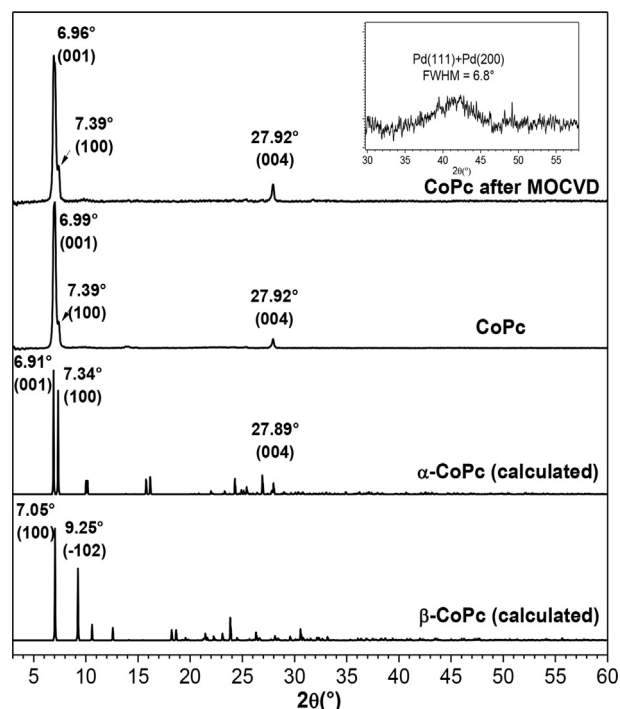


Fig. 2 – XRD patterns for the as-deposited CoPc film and the films after MOCVD experiment in comparison with the calculated powder patterns of α -CoPc and β -CoPc. The inset shows the magnified range from 30 to 50° 2 θ .

calculated powder patterns for α -CoPc [44] and β -CoPc [45] are also given for comparison. There are two known polymorphic phases of CoPc, and the calculated diffraction patterns of both of them contain strong diffraction peaks in this 2 θ region, viz. the (100) peak at 7.05° for β -CoPc and the (001) peak at 6.91° for α -CoPc. The XRD patterns of both films contain one strong diffraction peak, which indicates the presence of strong preferred orientation in the samples. The angular position of this peak is 6.99° 2 θ for the as-deposited CoPc and 6.96° for the heated CoPc/PdAu films, which is between the corresponding diffraction peaks on the calculated XRD patterns of α -CoPc and β -CoPc. However, the additional diffraction peaks at 7.39° and 27.92° observed on the XRD patterns of both films coincide

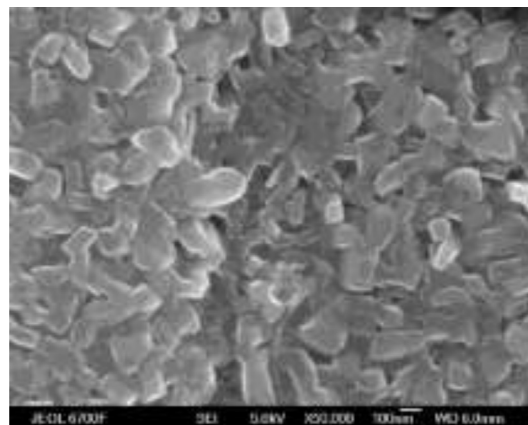


Fig. 3 – Microstructure of pure CoPc film.

well with the peaks (100) and (004) of α -CoPc. This fact and the comparison of XRD patterns with those of α -CoPc films deposited earlier under the same conditions [46] allows us to conclude that the CoPc films after MOCVD do not change their phase composition and consist only of the α -CoPc polymorph. Because of the small size and low amount of nanoparticles deposited by the pulsed CVD method only weak and wide diffraction peak is observed around 40° , which may correspond to the metallic Pd(111) and Pd(200).

To study the effect of bimetallic nanoalloys on the sensor response of CoPc films two types of heterostructures CoPc/Pd_{0.8}Au_{0.2} and CoPc/Pd_{0.2}Au_{0.8} were prepared and tested. The samples were deposited at the following conditions: $T_{\text{sub}} = 250^\circ\text{C}$; $T_{\text{vap}}([\text{Pd}(\text{hfac})_2]: [\text{Me}_2\text{Au}(\text{thd})]) = 75:65^\circ\text{C}$ and $60:75^\circ\text{C}$, accordingly. These compositions were selected to show the effect of dilution of Pd by Au using Pd-rich or Au-rich solid solutions as examples. Fig. 3 shows the microstructure of a CoPc film. The surface of the CoPc film consists of grains

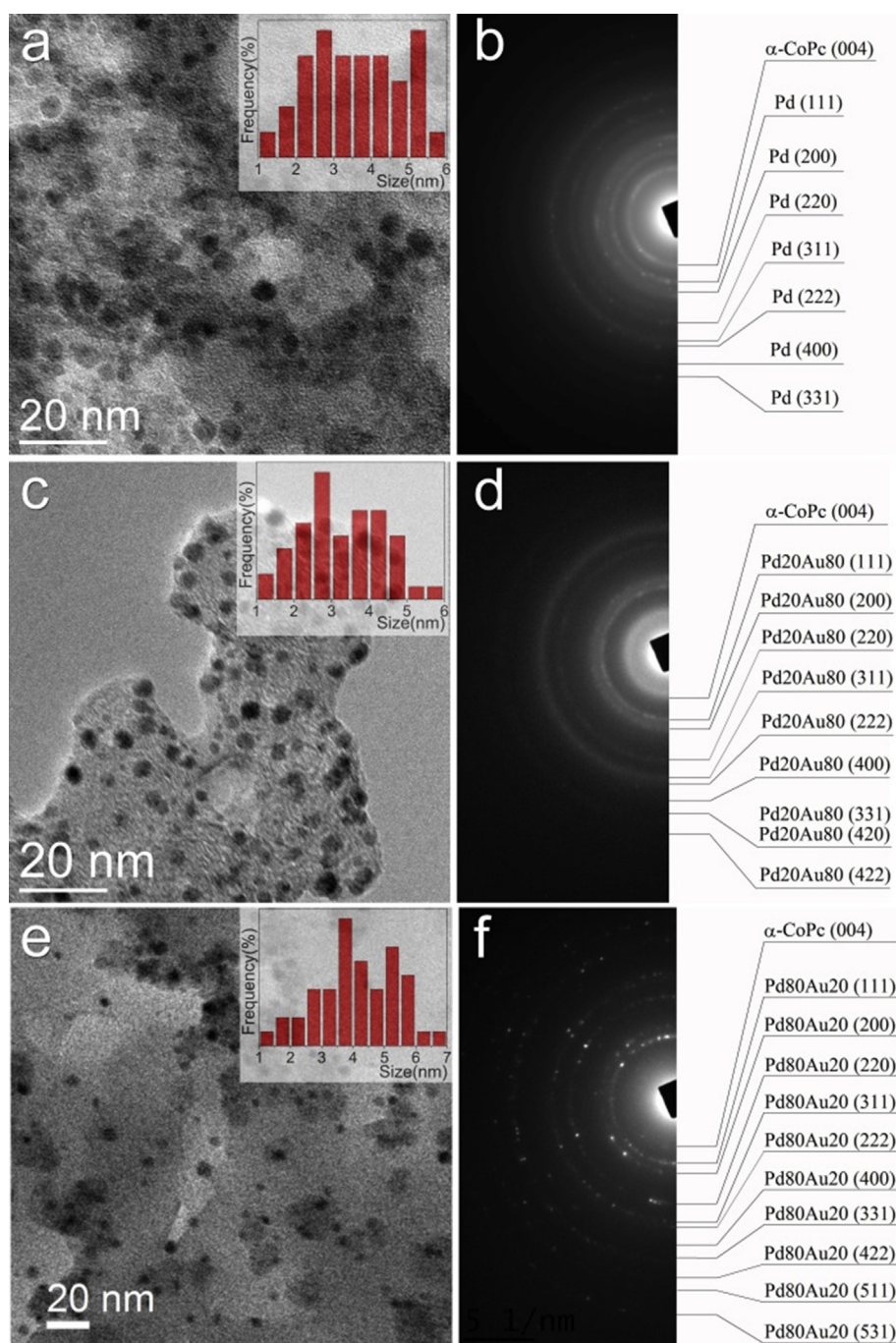


Fig. 4 – TEM images and corresponding electron diffraction patterns of CoPc/Pd (a, b), CoPc/Pd_{0.2}Au_{0.8} (c, d) and CoPc/Pd_{0.8}Au_{0.2} (e, f).

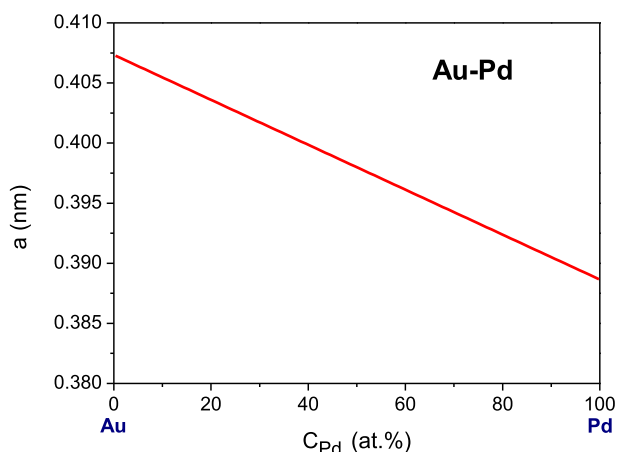


Fig. 5 – Lattice parameter of (Au,Pd) solid solutions vs. composition. Redrawn according to the data given in Ref. [47].

reaching a size of 70–100 nm. The sizes of the deposited metal nanoparticles were too small to obtain a high-quality SEM image, for this reason TEM was used to investigate them.

Fig. 4(a–f) shows the TEM images and corresponding electron diffraction patterns of CoPc/Pd, CoPc/Pd_{0.2}Au_{0.8} and CoPc/Pd_{0.8}Au_{0.2} heterostructures. The full size images of the electron diffraction patterns are given in Figs. S2–S4 (Supporting Information). The size distribution is broad and the nanoparticle size ranges from 1 to 7 nm in all investigated samples (see the insets on the TEM images). In Fig. 4b, the diffraction pattern contains sets of ring type reflections from Pd having polycrystalline structure with the fcc lattice (PDF4+ #00-046-1043) and α -CoPc (PDF4+ #00-055-1995). The introduction of Au leads to the formation of Au–Pd disordered solid solution (see Fig. 4d and f) according to the phase diagram. This can be tracked by changing the diameter of the diffraction reflections. The diameter of the diffraction rings decreases with the growing amount of gold as a result of the increase in the crystal lattice parameter without changes of the lattice type. The composition of the (Au,Pd) solid solution can be determined based on the linear dependence of the lattice parameter (Fig. 5). Thus, the following concentration ratios of the solid solutions were estimated from the electron diffraction patterns (see Fig. 4(d and f)): Pd_{0.2}Au_{0.8} ($a = 4.041 \text{ \AA}$) and Pd_{0.8}Au_{0.2} ($a = 3.928 \text{ \AA}$).

In general, the obtained phase composition of the bimetallic samples is in good correlation with the data of elemental analysis, which is the result of phase uniformity.

Investigation of the sensor response to hydrogen

It has earlier been shown that unsubstituted metal phthalocyanines, namely, PdPc, CoPc and VOPc, were used as sensing layers in chemiresistive sensors for hydrogen detection [33,34,48]. It is known that similarly to other p-type unsubstituted M(II)Pc, CoPc films are insulating in dark, high-vacuum environments and become semiconducting on exposure to air [49]. This air induced conductivity has been attributed to coordination of O₂ to surface MPC metal centers, forming superoxide adducts, which extract electrons,

generating charge carriers (holes) in the bulk film [50,51]. The initial resistance of the CoPc film was $7 \cdot 10^5 \text{ Ohm}$. The introduction of hydrogen to the gas flow cell leads to an increase of the resistance of CoPc films. A typical sensor response curve presented as $(R-R_0)/R_0$ for a CoPc film is given in Fig. 6.

The resistance-based sensing mechanism of semi-conducting sensors has been studied in the literature [52]. The commonly accepted mechanism is based on the variation of the surface electron depletion region due to the reaction between hydrogen and the chemisorbed oxygen on the surface. It has been assumed in the literature [53] that atmospheric oxygen absorbs at the air/MPC interface and at grain boundaries. It has been reported that the formation of charge-transfer complexes by coordination of O₂ to MPC at the air/phthalocyanine interface leads to the formation of oxidized MPC⁺ and O₂⁻ species and injection of hole charge carriers into the film's bulk [50,54]. The sensor layer is then exposed to hydrogen atmosphere and the hydrogen molecules react with the adsorbed oxygen species. This reaction is exothermic and results in the fast desorption of produced H₂O molecules from the surface [55]. Due to the released electrons a change of the resistance of the semiconductor is observed. Then the sensor is again purged with air, and its resistance returns to its original value.

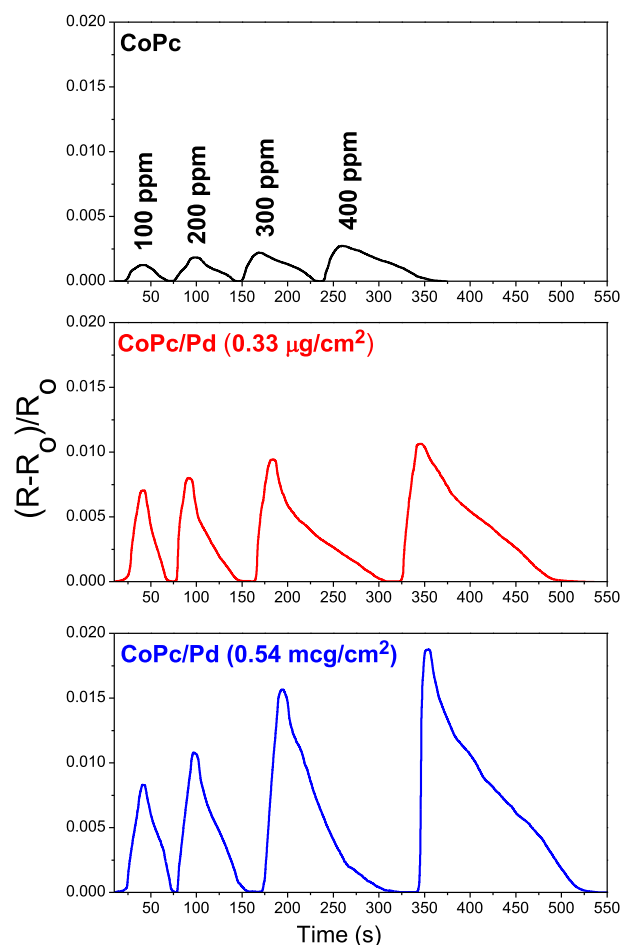


Fig. 6 – Sensor response of a CoPc film and CoPc/Pd heterostructures to hydrogen, measured at room temperature and RH 10%.

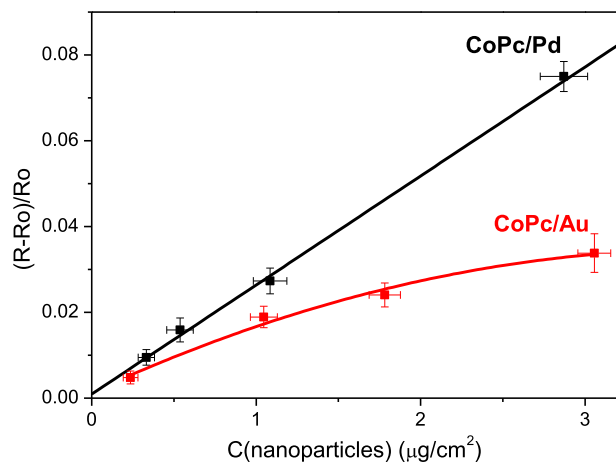


Fig. 7 – Dependence of the sensor response of CoPc/Au and CoPc/Pd heterostructures to hydrogen (300 ppm) on the concentration of nanoparticles, measured at room temperature and RH 10%.

Preliminary experiments have shown that cobalt phthalocyanine films exhibit the limit of hydrogen detection in air of about 100 ppm. For this reason, at this stage of the study, the range from 100 to 400 ppm of hydrogen was used to compare the effect of different nanoparticles on the sensor sensitivity and to select heterostructures with the best sensor characteristics. The sensor response of as-deposited CoPc films was compared with that of CoPc/Pd, CoPc/Au and CoPc/PdAu heterostructures. Deposition of Au and Pd nanoparticles onto the surface of a CoPc film led to the decrease in the resistance to $4 \cdot 10^5$ and $1 \cdot 10^5$ Ohm, respectively. This effect appears to be due to the charge transfer between nanoparticles and CoPc. Indeed, charge transfer from Au(100) single crystalline surface to Co central metal ion at CoPc/Au interface was demonstrated by Peisert et al. [56].

Typical sensor response curves for the CoPc/Pd heterostructures are given in Fig. 6 in comparison with that of a bare CoPc film. Similarly, to the case of CoPc films, the introduction

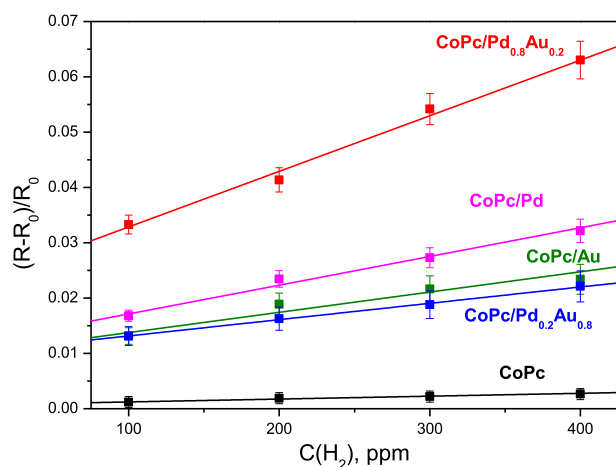


Fig. 8 – Dependence of the sensor response of a CoPc film and CoPc heterostructures with different metal nanoparticles on hydrogen concentration, measured at room temperature and RH 10%.

Table 1 – Values of the sensor response to hydrogen (300 ppm), response and recovery times for a CoPc film and heterostructures containing $1 \pm 0.09 \mu\text{g}/\text{cm}^2$ of nanoparticles.

Sample	$(R-R_0)/R_0$ at 300 ppm	
	H ₂	Response/recovery time (s)
bare CoPc	0.0022	20/70
CoPc/Pd	0.0273	30/170
CoPc/Au	0.0216	20/150
CoPc/ Pd _{0.8} Au _{0.2}	0.0556	27/180
CoPc/ Pd _{0.2} Au _{0.8}	0.0188	17/80

of hydrogen to the gas flow cell leads to an increase of the resistance of CoPc heterostructures with metal nanoparticles. It is important that all sensing layers demonstrate completely reversible sensor response to hydrogen even at room temperature. Deposition of Pd nanoparticles on the surface of CoPc films results in a noticeable increase of the sensor response to hydrogen. For instance, the responses of CoPc films containing 0.33 and $0.54 \mu\text{g}/\text{cm}^2$ of Pd nanoparticles to 400 ppm of H₂ increase by 4 and 7 times compared to the bare CoPc film. These results are in good agreement with the previously published work [34], in which Pd nanoparticles were deposited by the pulsed MOCVD method on the surface of VOPc thin films, however in that work the effect of Au nanoparticles on the sensor response to hydrogen was not investigated. Here the sensor response of CoPc heterostructures containing various amounts of Au nanoparticles was also studied. An increase of the concentration of Au nanoparticles from 0.01 to $3.06 \mu\text{g}/\text{cm}^2$ causes the 20-fold growth of the sensor response to hydrogen.

The dependence of the sensor response to hydrogen (300 ppm) on the concentration of Au and Pd nanoparticles in the CoPc-based heterostructures is shown in Fig. 7. In the case of heterostructures with Pd nanoparticles the dependence is linear in the investigated concentration range, while in the case of Au nanoparticles it deviates from the linear fit. The sensor response of the CoPc/Pd sample is higher than that in the case of CoPc/Au with a similar concentration of Au nanoparticles.

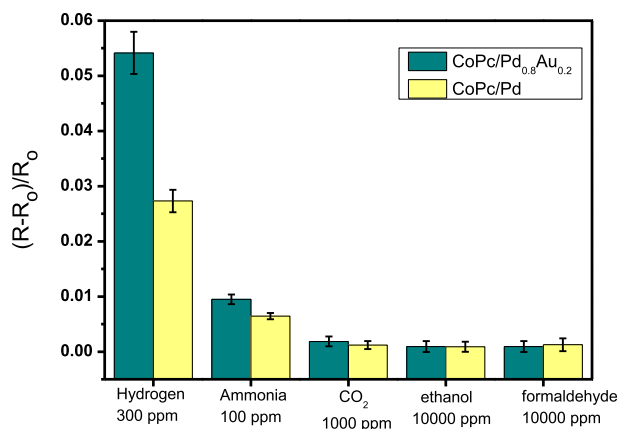


Fig. 9 – Sensitivity of CoPc/Pd and CoPc/Pd_{0.8}Au_{0.2} heterostructures to various analytes, measured at room temperature and RH 10%.

Table 2 – Sensor characteristics of various heterostructures or composite materials with bimetallic nanoparticles.

Active layer	Value of the sensor response	Concentration range, ppm	Temperature range, °C	Response/recovery time	Ref.
reduced graphene oxide/PtPd	46% (3000 ppm, r.t.)	50–8000	25–65	20 min/>35 min (3000 ppm)	[39]
ZnO nanorods/PtAu	25% (250 ppm, r.t.)	50–2000	20–200	–	[40]
porous polymer/PtPd	15.7% (40,000 ppm)	0.4–40000	room temperature (r.t.)	92 s/304 s (10,000 ppm H ₂)	[11]
CoPc/Pd _{0.8} Au _{0.2}	~6% (300 ppm)	100–400	room temperature	27 s/180s (300 ppm H ₂)	this work

For example, the response of CoPc/Pd containing 1.09 $\mu\text{g}/\text{cm}^2$ Pd nanoparticles is about 1.5 times higher than that of the CoPc/Au heterostructure with the concentration of Au nanoparticles of 1.05 $\mu\text{g}/\text{cm}^2$. This difference is even more significant at the higher concentrations of nanoparticles (Fig. 7).

It is believed [57,58] that the main reasons for the increase of gas sensitivity of composite materials based on semiconductor oxides and metal nanoparticles are the “spill-over” effect and/or increased surface area. Palladium is well known as a hydrogen-spillover metal and an effective catalyst for reactions owing to its strong affinity to hydrogen [59]. It is known that hydrogen cannot dissociate on Au(110) surface [60,61], whereas small gold clusters or narrow films deposited on different substrates show high catalytic activity [62–64]. H₂ adsorption mechanism on AuNPs was shown to depend strongly on the metal semiconductor support. For example, the dissociation of H₂ on Au/TiO₂, Au/Fe₂O₃ and Au/Al₂O₃ supported catalysts was found to occur at 300 K, and various chemical studies of the activation of H₂ on the Au sites were carried out [65,66]. Upon contact of hydrogen with the sensing layer, hydrogen molecules dissociate to the more active atomic hydrogen H in the presence of catalytic nanoparticles, which spills-over to the surface of a semiconductor film. Probably the same process occurs in the case of CoPc/Pd or CoPc/Au heterostructures. On the surface of CoPc, which is a p-type semiconductor [67,68], the formed atomic hydrogen interacts with adsorbed oxygen with the release of electrons, leading to the formation of hole depletion region and as a consequence, to an increase of the CoPc film resistance. In the case of CoPc/Au, the activation of H₂ and adsorption of H on Au are kinetically and thermodynamically less favorable [69] than in the case of Pd nanoparticles, leading to the less sensor response. Some researchers suggested that not all surface atoms of small gold clusters interact with hydrogen and hydrogen chemisorbs only on their edges and corners [70].

The dependence of the sensor response of CoPc heterostructures with different metal nanoparticles on hydrogen concentration (100–400 ppm) is presented in Fig. 8. The sensor responses of CoPc/Au and CoPc/Pd_{0.2}Au_{0.8} heterostructures are similar and 8–11 times higher than that of the bare CoPc film, but lower than in the case of heterostructures containing pure Pd nanoparticles. An increase of the content of Pd in bimetallic nanoparticles causes the growth of the response to hydrogen; in the case of CoPc/Pd_{0.8}Au_{0.2} it demonstrates 22–28 fold increase compared to that of bare CoPc layers, which is even higher than for CoPc/Pd heterostructures. The detection limit estimated as 3 s/m, where s is the standard deviation of the

sensor response to 100 ppm of hydrogen and *m* is the slope of the plot (Fig. 8, red line), was around 20 ppm for the CoPc/Pd_{0.8}Au_{0.2} heterostructure.

The superior properties of metal alloys are often considered both in terms of electronic and ensemble (geometric) effects [71,72]. Electronic effects refer to changes in catalytic properties due to electronic interactions between two components of a bimetallic alloy. Ensemble effects are related to the spatial distribution of the atomic sites where the components of alloy are located. Some reactions require large ensembles of reactive atoms to catalyze the transformation, and therefore stop when the active atom is dispersed over the entire inert lattice. Recent studies have shown that low amounts of Pd can promote H₂ dissociation and spillover onto the other surface. Lucci et al. [69] reported that Pd monomers on the Au (111) surface can activate hydrogen. At the same time, Baber et al. [73,74] found that the spillover effect was not observed for isolated Pd atoms on the surface of Au (111), but the larger ensembles of Pd were required. It was also noted that Pd tends to surround itself with host metal atoms and move to subsurface areas. We can suggest that in our case in the Pd_{0.2}Au_{0.8} solid solution containing the larger amount of Au, palladium can be encapsulated by gold atoms and not participate in the interaction with hydrogen. For this reason, the effect of Au nanoparticles and Pd_{0.2}Au_{0.8} was almost identical, as shown in Fig. 7. In contrast, in the case of Pd_{0.8}Au_{0.2} due to the larger amount of palladium the active Pd centers, which are necessary for hydrogen dissociation, appear to form on the surface of nanoparticles. It can be seen that the study of the atomic-scale structure of the surface of alloys is a crucial step for understanding this phenomenon, but this is the subject of a comprehensive separate study and will not be considered in this publication.

A comparison of the value of sensor response to hydrogen (300 ppm) as well as the response and recovery times for a CoPc film and heterostructures containing $1 \pm 0.09 \mu\text{g}/\text{cm}^2$ of nanoparticles is shown in Table 1.

It has already been mentioned that the detection of hydrogen is also an important issue for medicine, namely in hydrogen breath tests for the diagnostics of carbohydrate malabsorption [6]. The quite low limit of hydrogen detection makes the investigated CoPc/Pd_{0.8}Au_{0.2} heterostructures promising material for the preparation of active layers for the detection of hydrogen in exhaled air. In this connection, it was interesting to test the sensitivity of CoPc/Pd_{0.8}Au_{0.2} heterostructures to gases and vapors that may enter into the composition of exhaled air. To study selectivity of the

heterostructures their sensor response to ammonia (100 ppm), carbon dioxide (1000 ppm), ethanol (10,000 ppm) and formaldehyde (10,000 ppm) was measured. Fig. 9 shows the chemiresistive sensor response of CoPc/Pd and CoPc/Pd_{0.8}Au_{0.2} heterostructures to the above mentioned analytes. This diagram shows that the sensitivity of both heterostructures to hydrogen is much better than to carbon dioxide, ethanol, and formaldehyde, but ammonia can interfere with the determination of hydrogen in the gas mixtures.

Thus, heterostructures based on cobalt phthalocyanine and bimetallic nanoparticles CoPc/Pd_{0.8}Au_{0.2} have the best sensitivity to hydrogen compared to CoPc films and their heterostructures with monometallic Pd and Au nanoparticles.

There are only a few examples devoted to the study of chemiresistive sensors on the basis of heterostructures with bimetallic nanoparticles in the literature. Table 2 compares some characteristics of such sensors described in the literature with the results obtained in this work.

Conclusions

In this work, cobalt phthalocyanine films were modified with Pd and Au nanoparticles by a pulsed chemical vapor deposition method in order to enhance their sensitivity to hydrogen. The Pd-rich and Au-rich bimetallic PdAu nanoparticles were also obtained. The structural features and phase composition of the prepared heterostructures were studied by the techniques of XRD, TEM and electron diffraction. It was shown that the nanoparticle size ranged from 1 to 7 nm; the diffraction patterns contained sets of rings coming from Pd having polycrystalline structure with the fcc lattice and α -CoPc. The introduction of Au led to the formation of AuPd disordered solid solution. The effect of the amount and composition of metal nanoparticles on the chemiresistive sensor response of the prepared heterostructures to hydrogen (100–400 ppm) was investigated. It was shown that the sensor response of the investigated heterostructures to hydrogen (300 ppm) increased in the order CoPc (0.2%) < CoPc/Pd_{0.2}Au_{0.8} (1.9%) ~ CoPc/Au (2.2%) < CoPc/Pd (2.7%) < CoPc/Pd_{0.8}Au_{0.2} (5.6%). The detection limit of the CoPc/Pd_{0.8}Au_{0.2} heterostructures was estimated to be 20 ppm, which makes them a promising material for the preparation of active layers for the detection of hydrogen in the presence carbon dioxide and some volatile organic vapors, for example in exhaled air.

Declaration of competing interest

The authors declare that they have no known competing financial interests or personal relationships that could have appeared to influence the work reported in this paper.

Acknowledgments

The work on the synthesis of Au MOCVD precursor and deposition of gold nanoparticles on various surfaces were

funded by Russian Science Foundation (RSF) (research project № 20-15-00222). The TEM and electron diffraction investigations were conducted in the SFU Joint Scientific Center supported by the State assignment (#FSRZ-2020-0011) of the Ministry of Science and Higher Education of the Russian Federation.

Appendix A. Supplementary data

Supplementary data to this article can be found online at <https://doi.org/10.1016/j.ijhydene.2021.03.082>.

REFERENCES

- [1] Zhiznin SZ, Timokhov VM, Gusev AL. Economic aspects of nuclear and hydrogen energy in the world and Russia. *Int J Hydrogen Energy* 2020;45:31353–66. <https://doi.org/10.1016/j.ijhydene.2020.08.260>.
- [2] Forsberg CW. Future hydrogen markets for large-scale hydrogen production systems. *Int J Hydrogen Energy* 2007;32:431–9. <https://doi.org/10.1016/j.ijhydene.2006.06.059>.
- [3] Choi JH, Park T, Hur J, Cha HY. AlGaN/GaN heterojunction hydrogen sensor using ZnO-nanoparticles/Pd dual catalyst layer. *Sensor Actuator B Chem* 2020;325:128946. <https://doi.org/10.1016/j.snb.2020.128946>.
- [4] Hübert T, Boon-Brett L, Black G, Banach U. Hydrogen sensors - a review. *Sensor Actuator B Chem* 2011;157:329–52. <https://doi.org/10.1016/j.snb.2011.04.070>.
- [5] Sharma B, Sharma A, Kim JS. Recent advances on H₂ sensor technologies based on MOX and FET devices: a review. *Sensor Actuator B Chem* 2018;262:758–70. <https://doi.org/10.1016/j.snb.2018.01.212>.
- [6] Simrén M, Stotzer PO. Use and abuse of hydrogen breath tests. *Gut* 2006;55:297–303. <https://doi.org/10.1136/gut.2005.075127>.
- [7] Zhang H, Tao T, Li X, Bao Y, Xia X, Lourenço M, et al. Extending the detection range and response of TiO₂ based hydrogen sensors by surface defect engineering. *Int J Hydrogen Energy* 2020;45:18057–65. <https://doi.org/10.1016/j.ijhydene.2020.04.190>.
- [8] Kim S. Capacitance response characteristics of hydrogen sensor with tantalum oxide dielectric layer. *Int J Hydrogen Energy* 2018;43:19810. <https://doi.org/10.1016/j.ijhydene.2018.08.187>. –5.
- [9] Liu Y, Hao L, Gao W, Wu Z, Lin Y, Li G, et al. Hydrogen gas sensing properties of MoS₂/Si heterojunction. *Sensor Actuator B Chem* 2015;211:537–43. <https://doi.org/10.1016/j.snb.2015.01.129>.
- [10] Zhu Z, Liu C, Jiang F, Liu J, Liu G, Ma X, et al. Flexible fiber-shaped hydrogen gas sensor via coupling palladium with conductive polymer gel fiber. *J Hazard Mater* 2021;411:125008. <https://doi.org/10.1016/j.jhazmat.2020.125008>.
- [11] Koo WT, Kim Y, Kim S, Suh BL, Savagatrup S, Kim J, et al. Hydrogen sensors from composites of ultra-small bimetallic nanoparticles and porous ion-exchange polymers. *Inside Chem* 2020;6:2746–58. <https://doi.org/10.1016/j.chempr.2020.07.015>.
- [12] Ilnicka A, Lukaszewicz JP. Graphene-based hydrogen gas sensors: a review. *Processes* 2020;8:633. <https://doi.org/10.3390/PR8050633>.
- [13] Hu J, Sun Y, Xue Y, Zhang M, Li P, Lian K, et al. Highly sensitive and ultra-fast gas sensor based on CeO₂-loaded

- In₂O₃ hollow spheres for ppb-level hydrogen detection. *Sensor Actuator B Chem* 2018;257:469–76. <https://doi.org/10.1016/j.snb.2017.10.139>.
- [14] Darabpour M, Doroodmand MM. Fabrication of a glow discharge plasma-based ionization gas sensor using multiwalled carbon nanotubes for specific detection of hydrogen at parts per billion levels. *IEEE Sensor J* 2015;15:2391–8. <https://doi.org/10.1109/JSEN.2014.2369738>.
- [15] Mirzaei A, Yousefi HR, Falsafi F, Bonyani M, Lee JH, Kim JH, et al. An overview on how Pd on resistive-based nanomaterial gas sensors can enhance response toward hydrogen gas. *Int J Hydrogen Energy* 2019;44:20552–71. <https://doi.org/10.1016/j.ijhydene.2019.05.180>.
- [16] Chauhan PS, Bhattacharya S. Hydrogen gas sensing methods, materials, and approach to achieve parts per billion level detection: a review. *Int J Hydrogen Energy* 2019;44:26076–99. <https://doi.org/10.1016/j.ijhydene.2019.08.052>.
- [17] Luo Y, Zhang C, Zheng B, Geng X, Debligny M. Hydrogen sensors based on noble metal doped metal-oxide semiconductor: a review. *Int J Hydrogen Energy* 2017;42:20386–97. <https://doi.org/10.1016/J.IJHYDENE.2017.06.066>.
- [18] Gu H, Wang Z, Hu Y. Hydrogen gas sensors based on semiconductor oxide nanostructures. *Sensors* 2012;157:5517–50. <https://doi.org/10.3390/s120505517>.
- [19] Zhao J, Wang W, Liu Y, Ma J, Li X, Du Y, et al. Ordered mesoporous Pd/SnO₂ synthesized by a nanocasting route for high hydrogen sensing performance. *Sensor Actuator B Chem* 2011;160:604–8. <https://doi.org/10.1016/J.SNB.2011.08.035>.
- [20] Van Toan N, Viet Chien N, Van Duy N, Si Hong H, Nguyen H, Duc Hoa N, et al. Fabrication of highly sensitive and selective H₂ gas sensor based on SnO₂ thin film sensitized with micro-sized Pd islands. *J Hazard Mater* 2016;301:433–42. <https://doi.org/10.1016/j.jhazmat.2015.09.013>.
- [21] Sanger A, Kumar A, Kumar A, Chandra R. Highly sensitive and selective hydrogen gas sensor using sputtered grown Pd decorated MnO₂ nanowalls. *Sensor Actuator B Chem* 2016;234:8–14. <https://doi.org/10.1016/j.snb.2016.04.152>.
- [22] Jang B, Lee KY, Noh J-SS, Lee W. Nanogap-based electrical hydrogen sensors fabricated from Pd-PMMA hybrid thin films. *Sensor Actuator B Chem* 2014;193:530–5. <https://doi.org/10.1016/j.snb.2013.11.080>.
- [23] Szilágyi PÁ, Westerwaal RJ, van de Krol R, Geerlings H, Dam B. Metal–organic framework thin films for protective coating of Pd-based optical hydrogen sensors. *J Mater Chem C* 2013;1:8146–55. <https://doi.org/10.1039/c3tc31749h>.
- [24] Sayago I, Terrado E, Aleixandre M, Horrillo MC, Fernandez MJ, Lozano J, et al. Novel selective sensors based on carbon nanotube films for hydrogen detection. *Sensor Actuator B Chem* 2007;122:75–80. <https://doi.org/10.1016/j.snb.2006.05.005>.
- [25] Lu Y, Li J, Han J, Ng HT, Binder C, Partridge C, et al. Room temperature methane detection using palladium loaded single-walled carbon nanotube sensors. *Chem Phys Lett* 2004;391:344–8. <https://doi.org/10.1016/j.cplett.2004.05.029>.
- [26] Jaidev Baro M, Ramaprabhu S. Room temperature hydrogen gas sensing properties of mono dispersed platinum nanoparticles on graphene-like carbon-wrapped carbon nanotubes. *Int J Hydrogen Energy* 2018;43:16421–9. <https://doi.org/10.1016/j.ijhydene.2018.06.178>.
- [27] Hong J, Lee S, Seo J, Pyo S, Kim J, Lee T. A highly sensitive hydrogen sensor with gas selectivity using a PMMA membrane-coated Pd nanoparticle/single-layer graphene hybrid. *ACS Appl Mater Interfaces* 2015;7:3554–61. <https://doi.org/10.1021/am5073645>.
- [28] Cook MJ, Chambrier I. Phthalocyanine thin films: deposition and structural studies. *Porphyr. Handbook*, vol. 17. Elsevier; 2003. p. 37–127. <https://doi.org/10.1016/B978-0-08-092391-8.50008-X>.
- [29] Sun Q, Feng W, Yang P, You G, Chen Y. Highly selective room-temperature NO₂ sensors based on a fluoroalkoxy-substituted phthalocyanine. *New J Chem* 2018;42:6713–8. <https://doi.org/10.1039/c8nj00622a>.
- [30] Valli L. Phthalocyanine-based Langmuir-Blodgett films as chemical sensors. *Adv Colloid Interface Sci* 2005;116:13–44. <https://doi.org/10.1016/j.cis.2005.04.008>.
- [31] Jakubik WP, Urbańczyk MW, Kochowski S, Bodzenta J. Palladium and phthalocyanine bilayer films for hydrogen detection in a surface acoustic wave sensor system. *Sensor Actuator B Chem* 2003;96:321–8. [https://doi.org/10.1016/S0925-4005\(03\)00551-3](https://doi.org/10.1016/S0925-4005(03)00551-3).
- [32] Jakubik W, Krzywiecki M, Maciak E, Urbańczyk M. Bi-layer nanostructures of CuPc and Pd for resistance-type and SAW-type hydrogen gas sensors. *Sensor Actuator B Chem* 2012;82:265–71. <https://doi.org/10.1016/j.snb.2012.10.056>.
- [33] Nikolaeva NS, Parkhomenko RG, Klyamer DD, Shushanyan AD, Asanov IP, Morozova NB, et al. Bilayer structures based on metal phthalocyanine and palladium layers for selective hydrogen detection. *Int J Hydrogen Energy* 2017;42:28640–6. <https://doi.org/10.1016/j.ijhydene.2017.09.129>.
- [34] Klyamer D, Sukhikh A, Nikolaeva N, Morozova N, Basova T. Vanadyl phthalocyanine films and their hybrid structures with Pd nanoparticles: structure and sensing properties. *Sensors* 2020;20:1893. <https://doi.org/10.3390/s20071893>.
- [35] Ellert OG, Tsodikov MV, Nikolaev SA, Novotortsev VM. Bimetallic nanoalloys in heterogeneous catalysis of industrially important reactions: synergistic effects and structural organization of active components. *Russ Chem Rev* 2014;83:718. <https://doi.org/10.1070/rc2014v083n08abeh004432>.
- [36] Porter NS, Wu H, Quan Z, Fang J. Shape-control and electrocatalytic activity-enhancement of Pt-based bimetallic nanocrystals. *Acc Chem Res* 2013;46:1867–77. <https://doi.org/10.1021/ar3002238>.
- [37] Ockwig NW, Nenoff TM. Membranes for hydrogen separation. *Chem Rev* 2007;107:4078–110. <https://doi.org/10.1021/cr0501792>.
- [38] Hatlevik Ø, Gade SK, Keeling MK, Thoen PM, Davidson AP, Way JD. Palladium and palladium alloy membranes for hydrogen separation and production: history, fabrication strategies, and current performance. *Separ Purif Technol* 2010;73:59–64. <https://doi.org/10.1016/j.seppur.2009.10.020>.
- [39] Peng Y, Ye J, Zheng L, Zou K. The hydrogen sensing properties of Pt-Pd/reduced graphene oxide based sensor under different operating conditions. *RSC Adv* 2016;6:24880–8. <https://doi.org/10.1039/C5RA26618A>.
- [40] Fan F, Zhang J, Li J, Zhang N, Hong RR, Deng X, et al. Hydrogen sensing properties of Pt-Au bimetallic nanoparticles loaded on ZnO nanorods. *Sensor Actuator B Chem* 2017;241:895–903. <https://doi.org/10.1016/j.snb.2016.11.025>.
- [41] Dent CE, Leanstead RP. Phthalocyanines. Part IV. Copper phthalocyanines. *J Chem Soc* 1934:1027–30.
- [42] Zharkova GI, Zherikova KV, Morozova NB. Method of producing beta-diketonate of palladium (II). Patent RU 2 641 893 C1 2018.
- [43] Zharkova GI, Baidina IA, Igumenov IK. X-ray diffraction study of volatile complexes of dimethylgold(III) derived from symmetrical β-diketones. *J Struct Chem* 2006;47:1117–26. <https://doi.org/10.1007/s10947-006-0434-1>.
- [44] Ballirano P, Caminiti R, Ercolani C, Maras A, Orrù MA. X-ray powder diffraction structure reinvestigation of the α and β

- forms of cobalt phthalocyanine and kinetics of the $\alpha \rightarrow \beta$ phase transition. *J Am Chem Soc* 1998;120:12798–807. <https://doi.org/10.1021/ja973815p>.
- [45] Mason R, Williams GA, Fielding PE. Structural chemistry of phthalocyaninato-cobalt(II) and -manganese(II). *J Chem Soc, Dalton Trans* 1979;676–83. <https://doi.org/10.1039/DT9790000676>.
- [46] Sukhikh AS, Basova TV, Gromilov SA. Development of a procedure of X-ray study of thin layers by the example of cobalt phthalocyanine. *J Struct Chem* 2016;57:618–21. <https://doi.org/10.1134/S0022476616030227>.
- [47] Predel B. Phase equilibria, crystallographic and thermodynamic data of binary alloys: Ac-Au ... Au-Zr. In: Madelung O, editor. *Ac-Au – Au-Zr, Landolt-Börnstein, new series IV/5a*; 1991. <https://doi.org/10.1007/b20007>.
- [48] Dorovskikh SI, Vikulova ES, Nikolaeva NS, Shushanyan AD, Parkhomenko RG, Morozova NB, et al. Hybrid film structures based on palladium layers and metal phthalocyanines. *Sci Adv Mater* 2017;9:1087–92. <https://doi.org/10.1166/sam.2017.2794>.
- [49] Hiller S, Schlettwein D, Armstrong NR, Wöhrle D. Influence of surface reactions and ionization gradients on junction properties of F16PcZn. *J Mater Chem* 1998;8:945–54. <https://doi.org/10.1039/a707485i>.
- [50] Kerp HR, Westerduin KT, Van Veen AT, Van Faassen EE. Quantification and effects of molecular oxygen and water in zinc phthalocyanine layers. *J Mater Res* 2001;16:503–11. <https://doi.org/10.1557/JMR.2001.0073>.
- [51] Simon J, Andre J-J. *Molecular semiconductors. Photoelectrical properties and solar cells*. Berlin: Springer-Verlag Berlin Heidelberg; 1985. <https://doi.org/10.1007/978-3-642-70012-5>.
- [52] Soundarajan P, Schweighardt F. Hydrogen sensing and detection. In: Gupta RB, editor. *Hydrogen Fuel*; 2008. p. 624. <https://doi.org/10.1201/9781420045772.ch15>.
- [53] Gould RD. Structure and electrical conduction properties of phthalocyanine thin films. *Coord Chem Rev* 1996;156:237–74. [https://doi.org/10.1016/S0010-8545\(96\)01238-6](https://doi.org/10.1016/S0010-8545(96)01238-6).
- [54] de Haan A, Debliquy M, Decroly A. Influence of atmospheric pollutants on the conductance of phthalocyanine films. *Sensor Actuator B Chem* 1999;57:69–74. [https://doi.org/10.1016/S0925-4005\(99\)00137-9](https://doi.org/10.1016/S0925-4005(99)00137-9).
- [55] Gu HS, Wang Z, Hu YM. Hydrogen gas sensors based on semiconductor oxide nanostructures. *Sensors* 2012;12:5517–50. <https://doi.org/10.3390/S120505517>.
- [56] Peisert H, Uihlein J, Petraki F, Chassé T. Charge transfer between transition metal phthalocyanines and metal substrates: the role of the transition metal. *J Electron Spectrosc Relat Phenom* 2015;204:49–60. <https://doi.org/10.1016/j.ELSPEC.2015.01.005>.
- [57] Shahabuddin M, Umar A, Tomar M, Gupta V. Custom designed metal anchored SnO₂ sensor for H₂ detection. *Int J Hydrogen Energy* 2017;42:4597–609. <https://doi.org/10.1016/j.IJHYDENE.2016.12.054>.
- [58] Chang CM, Hon MH, Leu IC. Improvement in CO sensing characteristics by decorating ZnO nanorod arrays with Pd nanoparticles and the related mechanisms. *RSC Adv* 2012;2:2469–75. <https://doi.org/10.1039/c2ra01016j>.
- [59] Konda SK, Chen A. Palladium based nanomaterials for enhanced hydrogen spillover and storage. *Mater Today* 2016;19:100–8. <https://doi.org/10.1016/j.mattod.2015.08.002>.
- [60] Berger HF, Leisch M, Winkler A, Rendulic KD. A search for vibrational contributions to the activated adsorption of H₂ on copper. *Chem Phys Lett* 1990;175:425–8. [https://doi.org/10.1016/0009-2614\(90\)85558-T](https://doi.org/10.1016/0009-2614(90)85558-T).
- [61] Michelsen HA, Rettner CT, Auerbach DJ. On the influence of surface temperature on adsorption and desorption in the D₂/Cu(111) system. *Surf Sci* 1992;272:65–72. [https://doi.org/10.1016/0039-6028\(92\)91422-8](https://doi.org/10.1016/0039-6028(92)91422-8).
- [62] Claus P. Heterogeneously catalysed hydrogenation using gold catalysts. *Appl Catal Gen* 2005;291:222–9. <https://doi.org/10.1016/j.apcata.2004.12.048>.
- [63] Grirrane A, Corma A, García H. Gold-catalyzed synthesis of aromatic azo compounds from anilines and nitroaromatics. *Science* 2008;322:1661–4. <https://doi.org/10.1126/science.1166401> (80-).
- [64] Collins SSE, Cittadini M, Pecharromán C, Martucci A, Mulvaney P. Hydrogen spillover between single gold nanorods and metal oxide supports: a surface plasmon spectroscopy study. *ACS Nano* 2015;9:7846–56. <https://doi.org/10.1021/acsnano.5b02970>.
- [65] Venezia AM, Pantaleo G, Longo A, Di Carlo G, Casaletto MP, Liotta FL, et al. Relationship between structure and CO oxidation activity of ceria-supported gold catalysts. *J Phys Chem B* 2005;109:2821–7. <https://doi.org/10.1021/jp045928i>.
- [66] Boccuzzi F, Chiorino A, Manzoli M, Andreeva D, Tabakova T. FTIR study of the low-temperature water-gas shift reaction on Au/Fe₂O₃ and Au/TiO₂ catalysts. *J Catal* 1999;188:176–85. <https://doi.org/10.1006/jcat.1999.2636>.
- [67] Gounden D, Nombona N, van Zyl WE. Recent advances in phthalocyanines for chemical sensor, non-linear optics (NLO) and energy storage applications. *Coord Chem Rev* 2020;420:213359. <https://doi.org/10.1016/j.ccr.2020.213359>.
- [68] Yakuphanoglu F, Kandaz M, Yaraşır MN, Şenkal FB. Electrical transport and optical properties of an organic semiconductor based on phthalocyanine. *Phys B Condens Matter* 2007;393:235–8. <https://doi.org/10.1016/j.PHYSB.2007.01.007>.
- [69] Lucci FR, Darby MT, Mattera MFG, Ivimey CJ, Therrien AJ, Michaelides A, et al. Controlling hydrogen activation, spillover, and desorption with Pd-Au single-atom alloys. *J Phys Chem Lett* 2016;7:480–5. <https://doi.org/10.1021/acs.jpcllett.5b02400>.
- [70] Bus E, Miller JT, van Bokhoven JA. Hydrogenolysis of n-hexane on Al₂O₃-supported gold catalysts. *J Phys Chem B* 2005;109:14581–7. <https://doi.org/10.1021/jp051660z.CCC>.
- [71] Chen JG, Menning CA, Zellner MB. Monolayer bimetallic surfaces: experimental and theoretical studies of trends in electronic and chemical properties. *Surf Sci Rep* 2008;63:201–54. <https://doi.org/10.1016/j.surfrep.2008.02.001>.
- [72] Liu P, Nørskov JK. Ligand and ensemble effects in adsorption on alloy surfaces. *Phys Chem Chem Phys* 2001;3:3814–8. <https://doi.org/10.1039/b103525h>.
- [73] Baber AE, Tierney HL, Lawton TJ, Sykes ECH. An atomic-scale view of palladium alloys and their ability to dissociate molecular hydrogen. *ChemCatChem* 2011;3:607–14. <https://doi.org/10.1002/cctc.201000309>.
- [74] Tierney HL, Baber AE, Kitchin JR, Sykes ECH. Hydrogen dissociation and spillover on individual isolated palladium atoms. *Phys Rev Lett* 2009;103:246102. <https://doi.org/10.1103/PhysRevLett.103.246102>.